
H2G: Hierarchy-Aware Hyperbolic Grouping for 3D Scenes

ByungHa Ko^{1,2*} Youngmin Lee^{1,2*} Dong Hwan Kim^{1,2}

¹ Department of Computer Science and Engineering, Korea University

² Intelligence and Interaction Research Center, Korea Institute of Science and Technology

{rhqo123, aidi0724, gregorykim}@kist.re.kr

Abstract

Hierarchical 3D grouping aims to recover scene groups across multiple granularities, from fine object parts to complete objects, without relying on semantic labels or a fixed vocabulary. The main challenge is to transform 2D foundation-model cues into coherent hierarchy supervision and embed that hierarchy in a 3D representation. We propose H2G, a hyperbolic affinity field for hierarchical 3D grouping. Our method derives semantically organized tree supervision by interpreting foundation-model affinities through Dasgupta’s objective for similarity-based hierarchical clustering. This supervision is distilled into a single Lorentz hyperbolic feature field, whose geometry is well suited for tree-like branching structures. A hierarchy-aware objective aligns the field with fine-level assignments, coarse object structure, compact feature clusters, and LCA (Lowest Common Ancestor) ordering. This formulation represents multiple grouping levels in one feature space, enabling semantic hierarchical grouping grounded in 2D foundation-model knowledge.

1 Introduction

3D scene grouping is inherently hierarchical: the same point may belong to an object part, a whole object, or a larger object group depending on the desired granularity. Recent methods lift category-agnostic 2D masks, such as SAM[1] proposals, into NeRF-style[2] 3D fields for multi-view consistent grouping. The central challenge is not only to lift masks into 3D, but to organize overlapping and conflicting 2D proposals into a coherent hierarchy.

However, how these lifted masks should be organized into a hierarchy remains under-specified. GARField[3] resolves grouping ambiguity with a scale-conditioned affinity field, but this formulation ties hierarchy to depth-derived physical scale, which can be unreliable for large objects, partially observed objects, and amorphous background regions. It also requires repeated rendering over query scales. OmniSeg3D[4] and Ultrametric Feature Fields[5] avoid explicit scale queries through a unified feature-field representation, but the resulting hierarchies are still largely driven by mask-derived relations such as overlap, containment, or pixel-level correspondences among SAM-generated[1] masks. These relations provide useful boundary structure, but they do not necessarily align with semantic hierarchy.

Therefore, we propose H2G, a hyperbolic affinity field for hierarchical 3D grouping. Our method converts SAM[1] proposals into non-overlapping regions, computes DINO[6] descriptors for them, and constructs semantic affinity graphs over the resulting regions. Since their affinities are symmetric pairwise similarities rather than ordered hierarchy labels, we reconstruct them into tree supervision using a top-down construction motivated by Dasgupta’s objective[7] for similarity-based hierarchical clustering.

*Equal contribution.

The resulting 2D hierarchy is distilled into a single 3D grouping field in Lorentz hyperbolic space. The negative curvature of hyperbolic space provides a natural bias for representing branching structures with many descendants, while our hierarchy-aware objective combines leaf separation, root separation, cluster compactness, and LCA (Lowest Common Ancestor) ordering. This enables scale-free hierarchical 3D grouping from semantic relations, without depth-based scale queries or repeated scale-conditioned rendering.

Our contributions are threefold:

- We introduce a semantic 2D hierarchy construction that converts SAM[1] proposals and DINO[6] region affinities into tree supervision using a top-down procedure motivated by Dasgupta’s hierarchical clustering[7] objective.
- We formulate hierarchical 3D grouping as a scale-free Lorentz hyperbolic feature field, representing fine-to-coarse groups in a single embedding space without scale-conditioned rendering.
- We design a hierarchy-aware learning objective that combines leaf separation, root-level grouping, cluster compactness, and LCA-order preservation to align the 3D feature geometry with the constructed hierarchy.

The rest of this paper is organized as follows. Section 2 reviews neural feature fields, hierarchical 3D grouping, and hyperbolic representation learning. Section 3 describes the construction of 2D hierarchy supervision and its distillation into a Lorentz hyperbolic feature field. Section 4 presents quantitative and qualitative evaluations, followed by the conclusion.

2 Related work

Neural Feature Fields for 3D Scene Understanding Neural radiance fields(NeRF)[2] have been extended beyond RGB and density to store semantic, instance, language, and foundation-model features in 3D[8–14]. LERF[15], OpenScene[16], and OpenNeRF[17] align neural fields or 3D points with vision-language features for open-vocabulary scene understanding, while Contrastive Lift[18] shows that 2D segmentation cues can be lifted into 3D for instance segmentation. These works establish neural feature fields as a useful substrate for storing foundation-model signals in 3D. However, they typically support language queries, category retrieval, or flat instance labels, rather than class-agnostic hierarchical grouping. H2G instead uses feature fields to store hierarchy-aware grouping cues.

Hierarchical 3D Grouping from 2D Masks Closest to our setting are methods that lift multi-granular 2D masks, such as SAM[1] proposals, into view-consistent 3D representations[3–5, 19]. GARField[3] resolves grouping ambiguity with a scale-conditioned affinity field, Ultrametric Feature Fields[5] reveal hierarchy by thresholding feature distances, and OmniSeg3D[4] distills hierarchical 2D mask representations into a single 3D feature field. These methods show the importance of hierarchy, but differ in its source. Scale-conditioned inference requires repeated rendering across query scales, while mask overlap or containment may reflect proposal geometry more than semantic organization. H2G differs by reconstructing the 2D hierarchy from DINO[6] semantic affinities and embedding all grouping levels in a single Lorentz hyperbolic field.

Hyperbolic Representation Learning for Hierarchical Structure Hyperbolic representation learning[20–23] is well suited to tree-like data because hyperbolic volume grows exponentially with radius, allowing branching structures to be embedded with lower distortion than in Euclidean space. This geometry has been used for symbolic hierarchies, hierarchical clustering[24, 25], and vision-language representations[26, 27]. MERU[26] models visual-semantic specificity in hyperbolic image-text space, HypHC[24] uses hyperbolic geometry for hierarchical clustering and LCA recovery, and OpenHype[28] introduces hyperbolic embeddings into open-vocabulary radiance fields. These works motivate hyperbolic geometry as an inductive bias for hierarchy, but do not directly address dense class-agnostic 3D grouping. H2G applies this inductive bias to dense 3D grouping by learning ray-level Lorentz features with angular and LCA-order objectives.

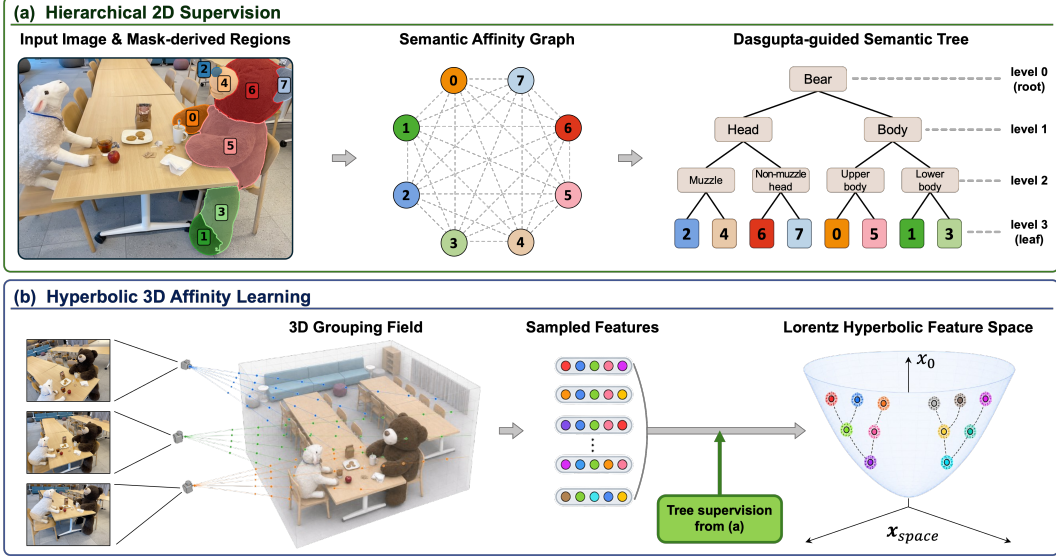


Figure 1: Overview of H2G. (a) Hierarchical 2D supervision converts mask-derived image regions into a semantic affinity graph using DINO region descriptors, then constructs a Dasgupta-guided semantic tree that provides leaf, root, and LCA relations. (b) Hyperbolic 3D affinity learning distills this tree supervision into a NeRF-style 3D grouping field whose rendered ray features lie in a Lorentz hyperbolic feature space. Text labels in the tree are illustrative; H2G does not use semantic class labels for supervision.

3 Method

Figure 1 summarizes the H2G pipeline. H2G first constructs image-wise hierarchy supervision from SAM[1] and DINO[6] cues, then distills it into a Lorentz hyperbolic feature field. The 2D stage converts overlapping SAM[1] proposals into non-overlapping leaf masks, organizes them into semantic trees using DINO[6] affinities, and provides leaf, root, and LCA relations for 3D learning.

3.1 Constructing 2D Hierarchy Supervision

Let $\{I^n\}_{n=1}^N$ denote the training images, where n is the image index. Given I^n , we first collect SAM[1] mask proposals and assign each proposal to its closest containing parent, defined as the smallest larger proposal whose containment ratio exceeds a threshold; proposals without parents become roots. Proposals sharing the same root are processed together, and their overlaps are resolved into fine non-overlapping leaf masks with unique ancestor paths. We denote one such leaf a by m_a^n .

Each leaf m_a^n receives a DINO[6] descriptor \mathbf{z}_a^n by average-pooling the DINO feature map Φ^n over its covered patches and applying ℓ_2 normalization:

$$\bar{\mathbf{z}}_a^n = \frac{1}{|\Omega_a^n|} \sum_{\mathbf{u} \in \Omega_a^n} \Phi^n(\mathbf{u}), \quad \mathbf{z}_a^n = \frac{\bar{\mathbf{z}}_a^n}{\|\bar{\mathbf{z}}_a^n\|_2}.$$

where Ω_a^n is the set of covered DINO[6] patch indices and \mathbf{u} indexes a DINO patch location. For each root-induced group indexed by i , we define an affinity graph $\mathcal{G}_i^n = (\mathcal{V}_{\text{leaf},i}^n, \mathcal{E}_i^n, \mathbf{W}_i^n)$, where $\mathcal{V}_{\text{leaf},i}^n$ contains the induced leaf vertices and \mathcal{E}_i^n fully connects them. The affinity matrix entry for an edge $(u, v) \in \mathcal{E}_i^n$ for each group i is $(\mathbf{W}_i^n)_{uv} = W_{uv}^n = \max(0, (\mathbf{z}_u^n)^\top \mathbf{z}_v^n)$. The graph is symmetric, whereas the desired supervision is an ordered tree. Dasgupta’s objective[7] for similarity-based hierarchical clustering provides the guiding principle for this conversion. For a tree \mathcal{T} and pairwise similarities \mathbf{W} , the objective assigns cost

$$\mathcal{C}(\mathcal{T}; \mathbf{W}) = \sum_{a < b} W_{ab} |\text{Leaf}(\text{LCA}_{\mathcal{T}}(a, b))|.$$

Here $\text{LCA}_{\mathcal{T}}(a, b)$ is the lowest common ancestor of leaves a and b , and $\text{Leaf}(v)$ is the set of leaf descendants under node v . This objective favors trees where high-affinity leaves meet in small subtrees. Dasgupta’s top-down approximation recursively applies an α -approximation algorithm for sparsest cut[7], but solving such cuts on our dense DINO[6] graphs is expensive. We therefore use recursive spectral bisection[29] as a practical surrogate. This surrogate gives comparable costs with substantially lower preprocessing time; we report this comparison in the Appendix C.

Starting from each affinity graph, we recursively split the current leaf set to build a tree. At each split, we compute the Fiedler vector of the normalized graph Laplacian of the induced DINO[6] affinity subgraph and divide leaves by its sign. Each split creates a virtual internal vertex whose children are the two resulting subtrees. Recursion continues until singleton leaves, with optional flattening of adjacent internal nodes for multi-way relations. Applying this process to all root-induced groups in image I^n yields a 2D hierarchy forest $\mathcal{T}^n = \{\mathcal{T}_i^n\}_{i=1}^{R_n}$, i.e., a collection of trees, one for each group.

Each tree $\mathcal{T}_i^n = (\mathcal{V}_{\mathcal{T},i}^n, \mathcal{E}_{\mathcal{T},i}^n)$ contains leaf vertices and virtual internal vertices, with $\mathcal{V}_{\mathcal{T},i}^n = \mathcal{V}_{\text{leaf},i}^n \cup \mathcal{V}_{\text{int},i}^n$. Thus, each labeled pixel or ray has a leaf label and a leaf-to-root ancestor chain $\mathcal{A}(y) = (y, \text{par}(y), \dots, \text{root}(y))$.

The DINO[6] graph is used only to construct the tree; 3D learning uses the resulting leaf labels, root labels, ancestor relations, and LCA relations as hierarchy supervision.

3.2 Hyperbolic 3D Affinity Learning

Hyperbolic Affinity Field The 2D hierarchy provides supervision for pixels or rays in each training view, but the goal is not to learn independent 2D segmentations for each view. Instead, H2G learns a multi-view consistent 3D grouping field. To this end, we use a NeRF-style[2] 3D feature field. The RGB/density branch provides scene geometry and volume-rendering weights, while the grouping branch predicts features at the same 3D sample locations. These 3D sample features are rendered along each ray to obtain a ray-level grouping feature aligned with the 2D hierarchy.

We use the D -dimensional Lorentz model $\mathbb{H}_c^D \subset \mathbb{R}^{D+1}$ with curvature parameter $c > 0$. For $\mathbf{x} = (x_0, \mathbf{x}_{\text{space}})$ and $\mathbf{y} = (y_0, \mathbf{y}_{\text{space}})$, the Lorentz inner product is $\langle \mathbf{x}, \mathbf{y} \rangle_L = -x_0 y_0 + \mathbf{x}_{\text{space}}^\top \mathbf{y}_{\text{space}}$, and $d_{\mathbb{H}}$ denotes the corresponding geodesic distance[21]. A Euclidean network output $\mathbf{u} \in \mathbb{R}^D$ is projected to the Lorentz hyperboloid by

$$\Pi_c(\mathbf{u}) = \left(\sqrt{\frac{1}{c} + \|\mathbf{u}\|_2^2}, \mathbf{u} \right) \in \mathbb{H}_c^D.$$

Concretely, for sample points $\mathbf{x}_{r,k}$ on ray r , a hashgrid encoder[30] E_ψ predicts sample features, and a projection head G_ψ maps the rendered feature to a Euclidean tangent parameter before hyperbolic projection. We aggregate the sample features over a high-weight sample set \mathcal{K}_r . Let $\tilde{w}_{r,k}$ denote normalized rendering weights detached from the gradient path. The ray-level feature and its hyperbolic projection are

$$\bar{\mathbf{h}}_r = \sum_{k \in \mathcal{K}_r} \tilde{w}_{r,k} E_\psi(\mathbf{x}_{r,k}), \quad \mathbf{s}_r = \Pi_c(G_\psi(\bar{\mathbf{h}}_r)) \in \mathbb{H}_c^D.$$

Here \mathbf{s}_r is the hyperbolic grouping feature for ray r , and it serves as the basic unit for the hierarchy-aware losses below.

Hierarchical Prototypes Direct pixel- or ray-wise contrastive learning over all pairs is costly and creates many redundant comparisons among rays from the same mask. Inspired by ProtoNCE [31], H2G treats each observed leaf mask as a prototype target: ray features assigned to the same leaf are aggregated into a single mask-level representative for contrastive supervision. This reduces the number of comparison targets and stabilizes learning by averaging noisy ray features within each leaf.

Let \mathcal{B} be a mini-batch of rays sampled from image I^n . Each ray $r \in \mathcal{B}$ has a leaf label y_r from the non-overlapping leaf partition, and the observed leaf set is $\mathcal{V}_{\mathcal{B}}^{\text{leaf}} = \{y_r \mid r \in \mathcal{B}\}$. For batches spanning multiple images, the same definitions are applied per image. We instantiate prototypes only for leaves in $\mathcal{V}_{\mathcal{B}}^{\text{leaf}}$. Virtual internal vertices are not prototype targets; they provide root and LCA metadata through the corresponding forest. To respect the Lorentz geometry, we aggregate ray features using the Klein-coordinate-based Einstein midpoint[32]:

$$\kappa(\mathbf{x}) = \frac{\mathbf{x}_{\text{space}}}{x_0}, \quad \text{E}_{\text{mid}}(\mathcal{X}) = \kappa^{-1} \left(\frac{\sum_{\mathbf{x} \in \mathcal{X}} \gamma(\mathbf{x}) \kappa(\mathbf{x})}{\sum_{\mathbf{x} \in \mathcal{X}} \gamma(\mathbf{x})} \right).$$

Here $\gamma(\mathbf{x}) = (1 - \|\kappa(\mathbf{x})\|_2^2)^{-1/2}$, and κ^{-1} denotes the inverse map from Klein coordinates to the Lorentz hyperboloid[32].

Using this operator, the prototype for each observed leaf label $\ell \in \mathcal{V}_{\mathcal{B}}^{\text{leaf}}$ is computed from its assigned ray features: $\mathbf{p}_{\ell} = \text{E}_{\text{mid}}(\{\mathbf{s}_r \mid y_r = \ell, r \in \mathcal{B}\})$. The resulting prototype set is $\mathcal{P}_{\mathcal{B}}^{\text{leaf}} = \{\mathbf{p}_{\ell} \mid \ell \in \mathcal{V}_{\mathcal{B}}^{\text{leaf}}\}$.

Angular Separation Loss Following the hyperbolic angular formulation of ATMG [27], H2G uses angular classification at two levels. The leaf-level loss aligns each ray feature with its assigned leaf prototype for fine discrimination, while the root-level loss aligns each leaf prototype with its root centroid for coarse group separation. Both losses use the same hyperbolic exterior angle. For the hyperbolic triangle formed by the origin O , a reference point \mathbf{p} , and a query point \mathbf{s} , we use the angle at \mathbf{p} , computed in the Lorentz model as

$$\theta(\mathbf{p}, \mathbf{s}) = \cos^{-1} \left(\frac{s_0 + p_0 c(\mathbf{p}, \mathbf{s})_L}{\|\mathbf{p}_{\text{space}}\|_2 \sqrt{(c(\mathbf{p}, \mathbf{s})_L)^2 - 1}} \right).$$

A smaller $\theta(\mathbf{p}, \mathbf{s})$ indicates stronger directional alignment. We use angle rather than hyperbolic distance so that semantic identity is organized mainly by direction, while radial position remains available for compactness and hierarchy ordering.

For leaf-level supervision, each ray feature \mathbf{s}_r is classified against the leaf prototypes observed in the current batch:

$$\mathcal{L}_{\text{leaf}} = -\frac{1}{|\mathcal{B}|} \sum_{r \in \mathcal{B}} \log \frac{\exp(-\theta(\mathbf{p}_{y_r}, \mathbf{s}_r)/\tau_{\text{leaf}})}{\sum_{v \in \mathcal{V}_{\mathcal{B}}^{\text{leaf}}} \exp(-\theta(\mathbf{p}_v, \mathbf{s}_r)/\tau_{\text{leaf}})}.$$

This loss separates leaves in angular space while aligning rays with their assigned leaf prototype.

Leaf-level separation alone does not guarantee that different root-level groups are well separated. The purpose of the root-level loss is not to classify individual rays again, but to make leaf-level representatives under the same root share a coarse group direction. Therefore, the classified queries are leaf prototypes rather than ray features. Let $\mathcal{R}_{\mathcal{B}} = \{\text{root}(\ell) \mid \ell \in \mathcal{V}_{\mathcal{B}}^{\text{leaf}}\}$ be the set of roots observed in the current batch. For each root $\rho \in \mathcal{R}_{\mathcal{B}}$, we compute a root centroid as the Einstein midpoint of its descendant leaf prototypes:

$$\mathbf{q}_{\rho} = \text{E}_{\text{mid}}(\{\mathbf{s}_r \mid \text{root}(y_r) = \rho, r \in \mathcal{B}\}).$$

Thus, each leaf prototype \mathbf{p}_{ℓ} uses its root $\text{root}(\ell)$ as the target class, and is classified against the root centroids $\{\mathbf{q}_{\rho}\}$:

$$\mathcal{L}_{\text{root}} = -\frac{1}{|\mathcal{V}_{\mathcal{B}}^{\text{leaf}}|} \sum_{\ell \in \mathcal{V}_{\mathcal{B}}^{\text{leaf}}} \log \frac{\exp(-\theta(\mathbf{q}_{\text{root}(\ell)}, \mathbf{p}_{\ell})/\tau_{\text{root}})}{\sum_{\rho \in \mathcal{R}_{\mathcal{B}}} \exp(-\theta(\mathbf{q}_{\rho}, \mathbf{p}_{\ell})/\tau_{\text{root}})}.$$

This term aligns leaf prototypes with their corresponding root centroids, encouraging leaves under the same root to share a coarse direction.

Compactness Loss Angle-based supervision separates semantic directions, but it does not control within-cluster spread. The compactness loss contracts only ray features that lie outside a margin around their assigned prototype.

For each ray feature \mathbf{s}_r , we penalize the excess hyperbolic distance to its assigned leaf prototype \mathbf{p}_{y_r} :

$$\mathcal{L}_{\text{comp}} = \frac{1}{|\mathcal{B}|} \sum_{r \in \mathcal{B}} (\text{ReLU}(d_{\mathbb{H}}(\mathbf{s}_r, \text{sg}(\mathbf{p}_{y_r})) - \epsilon))^2.$$

Here $\text{sg}(\cdot)$ denotes the stop-gradient operation, and ϵ is the compactness margin. Thus, rays within the margin receive no compactness gradient, while rays outside the margin are pulled toward the current prototype.

LCA Ordering Loss Angular losses separate leaves and roots, but they do not encode the merging order inside each tree. We adopt the LCA-order surrogate from HypHC [24] and apply it to tree-derived leaf prototypes in our 3D grouping field. LCA order therefore ranks prototype pairs by tree-derived ancestor depth. Let $\mathbf{k}_i = \kappa(\mathbf{p}_i)$ and $\mathbf{k}_j = \kappa(\mathbf{p}_j)$ be the Klein coordinates of two leaf prototypes. Since Klein geodesics are straight segments, the continuous LCA surrogate is approximated by the point on the segment closest to the origin:

$$t_{ij} = \text{clip}_{[0,1]} \left(-\frac{\mathbf{k}_i^\top (\mathbf{k}_j - \mathbf{k}_i)}{\|\mathbf{k}_j - \mathbf{k}_i\|_2^2} \right), \quad \hat{\mathbf{k}}_{ij} = \mathbf{k}_i + t_{ij}(\mathbf{k}_j - \mathbf{k}_i).$$

We use the hyperbolic distance from the origin to this point as a pairwise LCA-depth surrogate:

$$d_o(i, j) = \frac{1}{\sqrt{c}} \cosh^{-1} \left(\frac{1}{\sqrt{1 - \|\hat{\mathbf{k}}_{ij}\|_2^2}} \right).$$

Triples $(i, j, k) \in \mathcal{P}_{\text{LCA}}$ are sampled so that i and j come from the same parent, while k comes from a different sibling branch under the same grandparent. The desired relation is

$$d_o(i, j) > d_o(i, k), \quad d_o(i, j) > d_o(j, k).$$

This relation is optimized with a softmax ranking objective:

$$\mathcal{L}_{\text{LCA}} = -\frac{1}{|\mathcal{P}_{\text{LCA}}|} \sum_{(i,j,k) \in \mathcal{P}_{\text{LCA}}} \log \frac{\exp(d_o(i, j)/\tau_{\text{LCA}})}{\exp(d_o(i, j)/\tau_{\text{LCA}}) + \exp(d_o(i, k)/\tau_{\text{LCA}}) + \exp(d_o(j, k)/\tau_{\text{LCA}})}.$$

This loss enforces only relative LCA-depth ordering, preserving the merge order of the 2D hierarchy without regressing absolute pairwise distances.

Overall Objective The final training objective is the weighted sum of the four hierarchy losses and a max-norm regularizer:

$$\mathcal{L} = \lambda_{\text{leaf}} \mathcal{L}_{\text{leaf}} + \lambda_{\text{root}} \mathcal{L}_{\text{root}} + \lambda_{\text{comp}} \mathcal{L}_{\text{comp}} + \lambda_{\text{LCA}} \mathcal{L}_{\text{LCA}} + \lambda_{\text{norm}} \mathcal{L}_{\text{norm}}.$$

Rather than using a single contrastive objective for all hierarchy relations, H2G decomposes supervision into four complementary constraints: leaf-level angular separation, root-level angular grouping, within-leaf compactness, and LCA-order preservation. The max-norm regularizer only prevents Lorentz features from drifting too far from the origin and does not define hierarchy relations.

Through this decomposition, H2G distills the image-wise hierarchy obtained from SAM[1] and DINO[6] into a 3D hyperbolic affinity field. Each ray therefore receives a hyperbolic feature that reflects not only a leaf-level grouping label, but also root-level group structure and tree ordering.

H2G uses a NeRF[2] framework and training setup that closely follows GARField [3], while replacing scale-conditioned Euclidean grouping features with Lorentz features trained by our hierarchy-aware objective. Additional architecture and training details are provided in appendix A.

Table 1: Average 3D Completeness under view-wise (V) and level-wise (L) threshold selection. Scene-wise results are provided in Appendix B.3. * denotes methods evaluated under our reproduced setting.

Model	Fine		Medium		Coarse		Mean	
	V	L	V	L	V	L	V	L
SAM[1]	0.594	–	0.799	–	0.858	–	0.750	–
GARField[3]	0.846	–	0.877	–	0.917	–	0.880	–
SAM*	0.557	–	0.742	–	0.901	–	0.733	–
GARField*	0.824	0.823	0.607	0.587	0.815	0.784	0.749	0.731
Ours	0.848	0.840	0.813	0.809	0.844	0.828	0.835	0.826

4 Experiments

We evaluate whether H2G can identify and recover 3D groups across fine-to-coarse levels of detail within a single learned feature space.

4.1 Dataset

We evaluate on the GARField[3] scenes with hierarchical annotations. For 3D Completeness, each scene provides three evaluation views with query points corresponding to the same 3D location and ground-truth masks at two or three hierarchy levels. For group recall, each scene provides ground-truth hierarchical groups for best-match proposal evaluation.

Benchmark protocol Following the GARField 3D completeness protocol[3], we use query-conditioned mask retrieval across hierarchy levels. H2G renders each view once and obtains candidate masks by thresholding a tangent-space affinity map computed from the query feature, without scale input or per-level rendering. Additional evaluation details are provided in Appendix B.

For fair comparison, we compare H2G against baselines reproduced under the same evaluation protocol, denoted by *. Published SAM[1] and GARField[3] results are included only as references. We report OmniSeg3D[4] in Appendix B.3 because reproduced results are unavailable for one evaluation scene; the main table focuses on baselines with complete scene coverage.

4.2 3D Completeness

We report 3D completeness under two thresholding settings: view-wise selection, which chooses the best threshold for each view and level, and level-wise selection, which shares one threshold per hierarchy level across views. Mean values average the reported Fine, Medium, and Coarse entries, ignoring unavailable levels.

Table 1 shows that H2G achieves the best reproduced mean in both settings, improving over GARField* from 0.749 to 0.835 with view-wise thresholds and from 0.731 to 0.826 with level-wise thresholds. The gains are largest at the medium level, where semantic grouping is less directly tied to physical scale, supporting the role of semantic hierarchy supervision. The full scene-wise breakdown is reported in Appendix B.3; on `living_room`, GARField* remains slightly better in the view-wise mean.

We also introduce Cross-view Threshold Retention (CTR), the ratio between level-wise and view-wise 3D Completeness averaged over scenes. CTR measures how much performance is retained when one threshold is shared across views for each hierarchy level.

Table 2 shows that both methods retain most of their view-wise performance, while H2G has higher overall retention. Since both methods use a shared 3D representation, CTR should not be interpreted as multi-view consistency alone; rather, it reflects how consistently hierarchy levels are placed along each method’s inference variable. The higher mean CTR suggests that H2G calibrates medium and coarse levels more consistently in feature affinity, without relying on an explicit scale query.

Table 2: Cross-view Threshold Retention (CTR). Each value is computed as level-wise 3D Completeness divided by view-wise 3D Completeness for each scene, then averaged across scenes.

Method	Fine	Medium	Coarse	Mean
GARField*	0.998	0.967	0.959	0.975
Ours	0.990	0.995	0.978	0.988

Table 3: Group recall. Native uses all generated candidates. Budgeted rows sample at most K candidates without ground-truth information and average over 100 seeds. AUC values are normalized to the range of each metric.

Budget	GARField*			Ours		
	mIoU	$R@0.50$	$R@0.75$	mIoU	$R@0.50$	$R@0.75$
Candidates		2010.8			314.8	
Native	0.758	0.892	0.619	0.780	0.896	0.746
$K = 150$	0.368	0.373	0.210	0.541	0.580	0.413
$K = 500$	0.613	0.692	0.439	0.780	0.896	0.746
$K = 1000$	0.710	0.831	0.563	0.780	0.896	0.746
$K = 2000$	0.747	0.884	0.612	0.780	0.896	0.746
AUC ₅₀₀	0.427	0.457	0.274	0.596	0.662	0.521
AUC ₂₀₀₀	0.641	0.741	0.494	0.734	0.837	0.689

4.3 Group Recall

We follow the GARField group-recall protocol[3] to evaluate whether each method generates useful group candidates. GARField[3] accumulates candidates from scale-conditioned renderings, while H2G generates candidates from a single rendered feature field. We report native recall, fixed-budget recall, and budget-curve AUC; details are in Appendix B.

Table 3 shows that H2G produces a substantially smaller proposal pool while achieving higher native-pool mIoU and recall. H2G also outperforms GARField* at every evaluated proposal budget across mIoU, $R@0.50$, and $R@0.75$, and obtains higher budget-curve AUC. These results indicate that the learned hierarchy does not merely recover groups through dense proposal enumeration; instead, it concentrates useful hierarchical groups into a compact candidate pool.

4.4 Ablation study

Table 4 shows that angular separation is the most important component for fine-level grouping, while the root-level term controls the trade-off between local and coarse grouping. Removing the coarse term slightly improves Fine and Medium scores, but sharply reduces Coarse completeness, leading to a lower overall mean. This suggests that coarse supervision intentionally sacrifices some local thresholdability to preserve larger root-level groups. Compactness also improves the thresholdability of groups; LCA-order has a smaller effect on this metric but regularizes the relative merge order of leaf prototypes.

4.5 Qualitative results

Figures 2 and 3 visualize properties that are not fully captured by IoU-based scores. Compared with GARField[3], H2G produces clearer feature regions on large surfaces and more structured fine-grained clusters around object parts in cluttered or visually ambiguous regions. These qualitative differences suggest that part- and object-level groups form coherent neighborhoods in a single feature space, even when the final oracle IoU does not increase for every annotated group.

5 Limitations

H2G depends on the quality of its 2D supervision. Noisy SAM[1] proposals or unreliable DINO[6] affinities can produce imperfect hierarchy trees, especially for small, occluded, or visually ambiguous regions. Since trees are constructed per image, some cross-view inconsistencies may remain after 3D

Table 4: Ablation study on the proposed loss components.

Variant	Fine	Medium	Coarse	Mean
Full	0.848	0.813	0.844	0.835
w/o angle	0.631	0.774	0.830	0.745
w/o coarse	0.862	0.878	0.585	0.775
w/o compact	0.843	0.771	0.782	0.799
w/o LCA	0.847	0.806	0.839	0.831

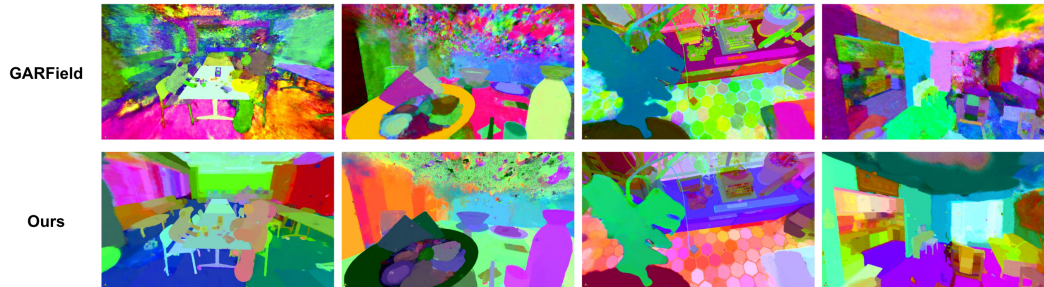


Figure 2: PCA (Principal component analysis) visualization of rendered grouping features. From left to right, the scenes are teatime, ramen, living_room, and bouquet. GARField is shown at scale 0.

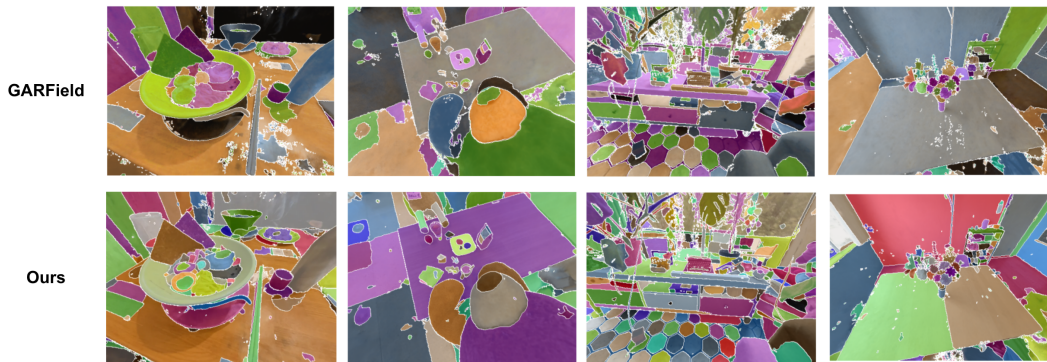


Figure 3: HDBSCAN clustering of rendered grouping features. From left to right, the scenes are ramen, teatime, living_room, and bouquet. GARField clusters are visualized from its recursive scale-sweep refinement, while H2G clusters are obtained from a single rendered feature field.

distillation. Finally, recursive spectral bisection is a practical approximation to hierarchy construction, and final mask extraction still requires thresholding or clustering in the learned feature space.

6 Conclusion

We presented H2G, a hierarchy-aware hyperbolic grouping field for 3D scenes. H2G reconstructs tree supervision from SAM[1] proposals and DINO[6] affinities, and distills it into a single Lorentz feature field through leaf, root, compactness, and LCA-order objectives. On the GARField 3D Completeness benchmark[3], H2G improves over reproduced baselines under both view-wise and level-wise threshold selection, especially at medium granularity. These results show that semantic hierarchy supervision and hyperbolic geometry provide an effective basis for hierarchical 3D grouping without scale-conditioned rendering.

References

- [1] Alexander Kirillov, Eric Mintun, Nikhila Ravi, Hanzi Mao, Chloe Rolland, Laura Gustafson, Tete Xiao, Spencer Whitehead, Alexander C Berg, Wan-Yen Lo, et al. Segment anything. In *Proceedings of the IEEE/CVF international conference on computer vision*, pages 4015–4026, 2023.
- [2] Ben Mildenhall, Pratul P Srinivasan, Matthew Tancik, Jonathan T Barron, Ravi Ramamoorthi, and Ren Ng. Nerf: Representing scenes as neural radiance fields for view synthesis. *Communications of the ACM*, 65(1):99–106, 2021.
- [3] Chung Min Kim, Mingxuan Wu, Justin Kerr, Ken Goldberg, Matthew Tancik, and Angjoo Kanazawa. Garfield: Group anything with radiance fields. In *Proceedings of the IEEE/CVF Conference on Computer Vision and Pattern Recognition*, pages 21530–21539, 2024.
- [4] Haiyang Ying, Yixuan Yin, Jinzhi Zhang, Fan Wang, Tao Yu, Ruqi Huang, and Lu Fang. Omnise3d: Omniversal 3d segmentation via hierarchical contrastive learning. In *Proceedings of the IEEE/CVF Conference on Computer Vision and Pattern Recognition*, pages 20612–20622, 2024.
- [5] Haodi He, Colton Stearns, Adam W Harley, and Leonidas J Guibas. View-consistent hierarchical 3d segmentation using ultrametric feature fields. In *European Conference on Computer Vision*, pages 268–286. Springer, 2024.
- [6] Oriane Siméoni, Huy V Vo, Maximilian Seitzer, Federico Baldassarre, Maxime Oquab, Cijo Jose, Vasil Khalidov, Marc Szafraniec, Seungeun Yi, Michaël Ramamonjisoa, et al. Dinov3. *arXiv preprint arXiv:2508.10104*, 2025.
- [7] Sanjoy Dasgupta. A cost function for similarity-based hierarchical clustering. In *Proceedings of the forty-eighth annual ACM symposium on Theory of Computing*, pages 118–127, 2016.
- [8] Suhani Vora*, Noha Radwan*, Klaus Greff, Henning Meyer, Kyle Genova, Mehdi S. M. Sajjadi, Etienne Pot, Andrea Tagliasacchi, and Daniel Duckworth. Nesf: Neural semantic fields for generalizable semantic segmentation of 3d scenes. *Transactions on Machine Learning Research*, 2022. <https://openreview.net/forum?id=ggPhsYCsm9>.
- [9] Sosuke Kobayashi, Eiichi Matsumoto, and Vincent Sitzmann. Decomposing nerf for editing via feature field distillation. *Advances in neural information processing systems*, 35:23311–23330, 2022.
- [10] Kunhao Liu, Fangneng Zhan, Jiahui Zhang, Muyu Xu, Yingchen Yu, Abdulmoteleb El Saddik, Christian Theobalt, Eric Xing, and Shijian Lu. Weakly supervised 3d open-vocabulary segmentation. *Advances in Neural Information Processing Systems*, 36:53433–53456, 2023.
- [11] Shuaifeng Zhi, Tristan Laidlow, Stefan Leutenegger, and Andrew J. Davison. In-place scene labelling and understanding with implicit scene representation. In *Proceedings of the IEEE/CVF International Conference on Computer Vision (ICCV)*, pages 15838–15847, October 2021.
- [12] Yawar Siddiqui, Lorenzo Porzi, Samuel Rota Bulò, Norman Müller, Matthias Nießner, Angela Dai, and Peter Kontschieder. Panoptic lifting for 3d scene understanding with neural fields. In *Proceedings of the IEEE/CVF Conference on Computer Vision and Pattern Recognition (CVPR)*, pages 9043–9052, June 2023.
- [13] Abhijit Kundu, Kyle Genova, Xiaoqi Yin, Alireza Fathi, Caroline Pantofaru, Leonidas J. Guibas, Andrea Tagliasacchi, Frank Dellaert, and Thomas Funkhouser. Panoptic neural fields: A semantic object-aware neural scene representation. In *Proceedings of the IEEE/CVF Conference on Computer Vision and Pattern Recognition (CVPR)*, pages 12871–12881, June 2022.
- [14] William Shen, Ge Yang, Alan Yu, Jansen Wong, Leslie Pack Kaelbling, and Phillip Isola. Distilled feature fields enable few-shot language-guided manipulation. In *7th Annual Conference on Robot Learning*, 2023.
- [15] Justin Kerr, Chung Min Kim, Ken Goldberg, Angjoo Kanazawa, and Matthew Tancik. Lerf: Language embedded radiance fields. In *Proceedings of the IEEE/CVF international conference on computer vision*, pages 19729–19739, 2023.
- [16] Songyou Peng, Kyle Genova, Chiyu Jiang, Andrea Tagliasacchi, Marc Pollefeys, Thomas Funkhouser, et al. Openscene: 3d scene understanding with open vocabularies. In *Proceedings of the IEEE/CVF conference on computer vision and pattern recognition*, pages 815–824, 2023.
- [17] Francis Engelmann, Fabian Manhardt, Michael Niemeyer, Keisuke Tateno, Marc Pollefeys, and Federico Tombari. OpenNeRF: Open Set 3D Neural Scene Segmentation with Pixel-Wise Features and Rendered Novel Views. In *International Conference on Learning Representations*, 2024.

- [18] Yash Bhalgat, Iro Laina, João F Henriques, Andrew Zisserman, and Andrea Vedaldi. Contrastive lift: 3d object instance segmentation by slow-fast contrastive fusion. In *Thirty-seventh Conference on Neural Information Processing Systems*, 2023.
- [19] Jiazhong Cen, Zanwei Zhou, Jiemin Fang, Chen Yang, Wei Shen, Lingxi Xie, Xiaopeng Zhang, and Qi Tian. Segment anything in 3d with nerfs. In *NeurIPS*, 2023.
- [20] Maximillian Nickel and Douwe Kiela. Poincaré embeddings for learning hierarchical representations. *Advances in neural information processing systems*, 30, 2017.
- [21] Maximillian Nickel and Douwe Kiela. Learning continuous hierarchies in the lorentz model of hyperbolic geometry. In *International conference on machine learning*, pages 3779–3788. PMLR, 2018.
- [22] Valentin Khruikov, Leyla Mirvakhabova, Evgeniya Ustinova, Ivan Oseledets, and Victor Lempitsky. Hyperbolic image embeddings. In *Proceedings of the IEEE/CVF conference on computer vision and pattern recognition*, pages 6418–6428, 2020.
- [23] Wei Peng, Tuomas Varanka, Abdelrahman Mostafa, Henglin Shi, and Guoying Zhao. Hyperbolic deep neural networks: A survey. *IEEE Transactions on Pattern Analysis and Machine Intelligence*, 44(12):10023–10044, 2022.
- [24] Ines Chami, Albert Gu, Vaggos Chatziafratis, and Christopher Ré. From trees to continuous embeddings and back: Hyperbolic hierarchical clustering. *Advances in neural information processing systems*, 33:15065–15076, 2020.
- [25] Teng Long and Nanne van Noord. Cross-modal scalable hyperbolic hierarchical clustering. In *Proceedings of the IEEE/CVF international conference on computer vision*, pages 16655–16664, 2023.
- [26] Karan Desai, Maximilian Nickel, Tanmay Rajpurohit, Justin Johnson, and Shanmukha Ramakrishna Vedantam. Hyperbolic image-text representations. In *International Conference on Machine Learning*, pages 7694–7731. PMLR, 2023.
- [27] Sameera Ramasinghe, Violetta Shevchenko, Gil Avraham, and Ajanthan Thalaiyasingam. Accept the modality gap: An exploration in the hyperbolic space. In *Proceedings of the IEEE/CVF Conference on Computer Vision and Pattern Recognition*, pages 27263–27272, 2024.
- [28] Lisa Weijler, Sebastian Koch, Fabio Poiesi, Timo Ropinski, and Pedro Hermosilla. Openhype: Hyperbolic embeddings for hierarchical open-vocabulary radiance fields. *NeurIPS*, 2025.
- [29] Miroslav Fiedler. A property of eigenvectors of nonnegative symmetric matrices and its application to graph theory. *Czechoslovak mathematical journal*, 25(4):619–633, 1975.
- [30] Thomas Müller, Alex Evans, Christoph Schied, and Alexander Keller. Instant neural graphics primitives with a multiresolution hash encoding. *ACM Trans. Graph.*, 41(4):102:1–102:15, July 2022.
- [31] Junnan Li, Pan Zhou, Caiming Xiong, and Steven C.H. Hoi. Prototypical contrastive learning of unsupervised representations. In *ICLR*, 2021.
- [32] Abraham Albert Ungar. *Analytic hyperbolic geometry: Mathematical foundations and applications*. World Scientific, 2005.
- [33] Tsung-Yi Lin, Michael Maire, Serge Belongie, James Hays, Pietro Perona, Deva Ramanan, Piotr Dollár, and C. Lawrence Zitnick. Microsoft coco: Common objects in context. In David Fleet, Tomas Pajdla, Bernt Schiele, and Tinne Tuytelaars, editors, *Computer Vision – ECCV 2014*, pages 740–755, Cham, 2014. Springer International Publishing.
- [34] Ricardo J. G. B. Campello, Davoud Moulavi, and Joerg Sander. Density-based clustering based on hierarchical density estimates. In Jian Pei, Vincent S. Tseng, Longbing Cao, Hiroshi Motoda, and Guandong Xu, editors, *Advances in Knowledge Discovery and Data Mining*, pages 160–172, Berlin, Heidelberg, 2013. Springer Berlin Heidelberg.

A Implementation details

We train H2G in two stages. First, we optimize the RGB radiance field for 30k iterations. We then freeze the RGB field, proposal networks, and camera optimizer, and train only the semantic grouping field for 20k iterations with hierarchy supervision enabled from the beginning.

For 2D hierarchy preprocessing, SAM[1] masks are generated in automatic mode and sorted by area. We form top-down proposal groups using a containment threshold of 0.8, convert overlapping masks into non-overlapping leaf masks by assigning pixels to the smallest covering mask, and apply morphological closing and connected-component filtering. DINO[6] descriptors are mean-pooled over the resulting leaf masks, and neighboring internal nodes with a small height gap can be flattened to represent multi-way relations.

The semantic hash grid[30] is warm-started from the RGB hash grid[30] learned in the first stage. The grouping feature dimension is 256. During semantic training, we sample 8192 rays from one image per iteration and optimize the semantic branch with Adam. The initial learning rate is 10^{-3} , the final learning rate is 10^{-4} , warmup lasts 1000 steps, weight decay is 10^{-6} , and gradients are clipped with maximum norm 1.0. The hierarchy loss is weighted by 0.5. Unless otherwise stated, we use compactness weight 1.0, root coarse weight 2.0, LCA order weight 0.05, LCA temperature 0.5, leaf angle temperature 0.22, and root temperature 0.20. All experiments were run on a local workstation equipped with NVIDIA RTX 3090 GPUs, each with 24GB VRAM. Generating the 2D hierarchy supervision takes approximately 30 minutes per scene, and hierarchy-supervised grouping-field training takes approximately 20 minutes per scene.

Reproduced baselines. In the main experiments, we include published SAM[1] and GARField[3] results as references, but base all direct comparisons on reproduced baselines evaluated under the same protocol as H2G. We used the same GARField[3] evaluation scenes and query annotations, and matched the available SAM ViT-H checkpoint and mask-generation settings as closely as possible. We observed differences from the published results, which can arise from checkpoint availability, implementation details, environment differences, and the sensitivity of scale-conditioned grouping to ambiguous same-scale groups. Therefore, reproduced results are marked with *, and our claims are made against these reproduced baselines rather than against the reference results.

B Evaluation Details

B.1 3D Completeness Protocol

For each scene, we evaluate H2G using the annotated camera poses, query pixels, and COCO-format[33] hierarchy masks provided by the GARField 3D Completeness benchmark[3]. Each evaluation view contains a query pixel corresponding to the same 3D point, and each hierarchy level provides a ground-truth mask that contains the query. H2G renders the RGB image and grouping feature field once for each evaluation camera; unlike scale-conditioned methods, the renderer does not receive a separate scale or hierarchy-level input.

For the reported H2G scores, we use tangent-space query affinity. Let $f(p)$ be the rendered Lorentz feature at pixel p , and let q be the query pixel. Features are mapped to the tangent space at the origin with the Lorentz logarithmic map, and the query-conditioned score is computed as

$$z(p) = \log_0(f(p); c), \quad \text{score}_q(p) = \exp(-\|z(p) - z(q)\|_2^2).$$

A candidate mask for threshold t is $M_q(t) = \{p \in I \mid \text{score}_q(p) \geq t\}$. In the view-wise setting, we sweep 1000 linearly spaced thresholds in $[0.0, 0.99]$ independently for each evaluation view and annotated hierarchy level, then select the threshold that maximizes IoU with the corresponding ground-truth mask. The per-level score is the mean IoU over the three evaluation views. In the level-wise setting, we use the same tangent affinity maps but select one threshold per hierarchy level by maximizing the total IoU across all evaluation views, then evaluate every view at that level with the shared threshold. The reported mean averages the available Fine, Medium, and Coarse levels for each scene.

B.2 Group Recall Protocol

For H2G group recall, we render the evaluation view once and project the rendered Lorentz features to the tangent space at the origin. Candidate groups are then generated by recursively splitting the current leaf regions with HDBSCAN[34] in tangent space. We sweep the HDBSCAN cluster-selection epsilon from 0.50 down to 0.002 using a coarse-to-fine schedule: 0.05 steps from 0.50 to 0.20, 0.025 steps from 0.20 to 0.10, 0.01–0.015 steps from 0.10 to 0.04, 0.005 steps from 0.04 to 0.02, and smaller steps down to 0.002. At each epsilon, every current leaf with at least 30 pixels is clustered with HDBSCAN using `min_samples=30` and `min_cluster_size=30`. Noise pixels are assigned to the nearest non-noise cluster, and clusters with fewer than 30 pixels are discarded. Each accepted cluster is added as a candidate group and becomes a new leaf for subsequent, smaller-epsilon splits. Candidate generation is capped at 10,000 nodes, although this cap is not reached in our reported results.

For native group recall, all generated candidates are used. For budgeted recall, we evaluate proposal budgets $K \in \{50, 100, 150, 180, 300, 500, 750, 1000, 1500, 2000\}$. When a scene has fewer than K H2G candidates, all available candidates are used. Random budget sampling is repeated for 100 seeds with seed 0 as the base seed. For each ground-truth group, we report the best IoU over the selected candidate set, and compute mIoU, $R@0.50$, and $R@0.75$. The reported AUC values are normalized areas under the corresponding budget curves.

B.3 Full 3D Completeness Results

Table 5: Scene-wise 3D Completeness under view-wise (V) and level-wise (L) threshold selection. * denotes methods evaluated under our reproduced setting.

Scene	Model	Fine		Medium		Coarse		Mean	
		V	L	V	L	V	L	V	L
teatime	SAM[1]	0.816	–	–	–	0.973	–	0.895	–
	GARField[3]	0.927	–	–	–	0.979	–	0.953	–
	SAM*	0.714	–	–	–	0.976	–	0.845	–
	GARField*	0.893	0.893	–	–	0.754	0.633	0.824	0.763
	OmniSeg3D*	0.306	0.281	–	–	0.249	0.192	0.278	0.237
	Ours	0.931	0.928	–	–	0.973	0.972	0.952	0.950
bouquet	SAM[1]	0.174	–	0.735	–	0.761	–	0.557	–
	GARField[3]	0.760	–	0.816	–	0.854	–	0.810	–
	SAM*	0.126	–	0.584	–	0.831	–	0.514	–
	GARField*	0.785	0.785	0.617	0.563	0.632	0.632	0.678	0.660
	OmniSeg3D*	0.388	0.388	0.702	0.697	0.267	0.254	0.453	0.447
	Ours	0.753	0.748	0.862	0.858	0.635	0.601	0.750	0.736
ramen	SAM[1]	0.533	–	0.747	–	0.926	–	0.735	–
	GARField[3]	0.792	–	0.907	–	0.955	–	0.885	–
	SAM*	0.538	–	0.916	–	0.944	–	0.799	–
	GARField*	0.754	0.749	0.507	0.507	0.937	0.936	0.733	0.731
	OmniSeg3D*	0.484	0.483	0.813	0.800	0.190	0.161	0.496	0.481
	Ours	0.823	0.806	0.916	0.913	0.838	0.811	0.859	0.843
living_room	SAM[1]	0.853	–	0.742	–	0.886	–	0.827	–
	GARField[3]	0.905	–	0.807	–	0.944	–	0.885	–
	SAM*	0.850	–	0.727	–	0.851	–	0.809	–
	GARField*	0.863	0.863	0.698	0.690	0.936	0.935	0.832	0.829
	OmniSeg3D*	–	–	–	–	–	–	–	–
	Ours	0.883	0.876	0.660	0.656	0.929	0.928	0.824	0.820
mean	SAM[1]	0.594	–	0.799	–	0.858	–	0.750	–
	GARField[3]	0.846	–	0.877	–	0.917	–	0.880	–
	SAM*	0.557	–	0.742	–	0.901	–	0.733	–
	GARField*	0.824	0.823	0.607	0.587	0.815	0.784	0.749	0.731
	OmniSeg3D*	–	–	–	–	–	–	–	–
	Ours	0.848	0.840	0.813	0.809	0.844	0.828	0.835	0.826

B.4 Full Group Recall Results

Table 6: Scene-wise group recall on the GARField group annotation benchmark. Budgeted rows use random proposal sampling averaged over 100 seeds. AUC is computed from the random budget curve with an origin point at zero budget.

Scene	Budget	GARField*			Ours		
		mIoU	$R@0.50$	$R@0.75$	mIoU	$R@0.50$	$R@0.75$
bouquet	Candidates	2220			310		
	Native	0.717	0.929	0.429	0.719	0.786	0.643
	$K = 50$	0.217	0.185	0.069	0.253	0.214	0.111
	$K = 100$	0.352	0.341	0.139	0.419	0.391	0.231
	$K = 150$	0.430	0.440	0.176	0.533	0.533	0.349
	$K = 180$	0.463	0.483	0.202	0.558	0.556	0.366
	$K = 300$	0.588	0.683	0.280	0.710	0.772	0.626
	$K = 500$	0.650	0.792	0.347	0.719	0.786	0.643
	$K = 750$	0.688	0.878	0.402	0.719	0.786	0.643
	$K = 1000$	0.699	0.902	0.411	0.719	0.786	0.643
	$K = 1500$	0.712	0.927	0.424	0.719	0.786	0.643
	$K = 2000$	0.716	0.929	0.429	0.719	0.786	0.643
	AUC ₅₀₀	0.479	0.537	0.224	0.564	0.591	0.446
	AUC ₂₀₀₀	0.645	0.811	0.365	0.680	0.737	0.594
living_room	Candidates	3256			342		
	Native	0.724	0.778	0.667	0.722	0.889	0.667
	$K = 50$	0.067	0.057	0.038	0.186	0.186	0.118
	$K = 100$	0.125	0.117	0.077	0.329	0.361	0.234
	$K = 150$	0.190	0.172	0.120	0.419	0.481	0.311
	$K = 180$	0.211	0.197	0.130	0.487	0.571	0.383
	$K = 300$	0.323	0.309	0.224	0.662	0.800	0.596
	$K = 500$	0.425	0.417	0.320	0.722	0.889	0.667
	$K = 750$	0.521	0.538	0.449	0.722	0.889	0.667
	$K = 1000$	0.582	0.621	0.509	0.722	0.889	0.667
	$K = 1500$	0.652	0.706	0.606	0.722	0.889	0.667
	$K = 2000$	0.679	0.743	0.638	0.722	0.889	0.667
	AUC ₅₀₀	0.254	0.243	0.176	0.514	0.613	0.442
	AUC ₂₀₀₀	0.512	0.540	0.447	0.670	0.820	0.610
ramen	Candidates	1438			366		
	Native	0.773	0.864	0.682	0.813	0.909	0.773
	$K = 50$	0.255	0.223	0.145	0.270	0.237	0.160
	$K = 100$	0.358	0.329	0.222	0.430	0.405	0.269
	$K = 150$	0.433	0.400	0.286	0.538	0.537	0.376
	$K = 180$	0.478	0.448	0.330	0.605	0.616	0.447
	$K = 300$	0.549	0.543	0.399	0.757	0.830	0.666
	$K = 500$	0.638	0.651	0.505	0.813	0.909	0.773
	$K = 750$	0.707	0.750	0.587	0.813	0.909	0.773
	$K = 1000$	0.745	0.802	0.631	0.813	0.909	0.773
	$K = 1500$	0.773	0.864	0.682	0.813	0.909	0.773
	$K = 2000$	0.773	0.864	0.682	0.813	0.909	0.773
	AUC ₅₀₀	0.471	0.458	0.338	0.609	0.647	0.508
	AUC ₂₀₀₀	0.675	0.723	0.563	0.762	0.844	0.706
teatime	Candidates	1129			241		
	Native	0.819	1.000	0.700	0.869	1.000	0.900
	$K = 50$	0.203	0.194	0.105	0.315	0.328	0.242
	$K = 100$	0.357	0.377	0.212	0.519	0.576	0.434
	$K = 150$	0.419	0.481	0.258	0.673	0.769	0.614
	$K = 180$	0.489	0.560	0.319	0.733	0.836	0.698
	$K = 300$	0.610	0.720	0.445	0.869	1.000	0.900
	$K = 500$	0.738	0.907	0.582	0.869	1.000	0.900
	$K = 750$	0.794	0.977	0.662	0.869	1.000	0.900
	$K = 1000$	0.816	0.998	0.699	0.869	1.000	0.900
	$K = 1500$	0.819	1.000	0.700	0.869	1.000	0.900
	$K = 2000$	0.819	1.000	0.700	0.869	1.000	0.900
	AUC ₅₀₀	0.506	0.591	0.359	0.699	0.797	0.689
	AUC ₂₀₀₀	0.732	0.889	0.602	0.826	0.949	0.847

C Spectral Bisection Analysis

Dasgupta’s objective motivates a recursive top-down construction in which each branch is split by a sparse-cut approximation. In our setting, however, each proposal group induces a dense DINO affinity graph, making exact recursive sparsest cut expensive as the number of leaves grows. We therefore use recursive spectral bisection in the main pipeline and compare it with exact sparsest cut on the same DINO graphs.

Figure 4 shows that spectral bisection closely tracks exact sparsest cut in normalized Dasgupta cost across max-leaf settings. The relative cost gap remains small: the median gap is below 0.15%, and the mean gap stays below about 0.22% even at the largest setting. This indicates that the surrogate preserves the tree quality measured by Dasgupta’s objective.

The computational difference is much larger. Exact recursive sparsest cut grows rapidly with the max-leaf setting, reaching over 10^2 seconds in total preprocessing time, whereas spectral bisection

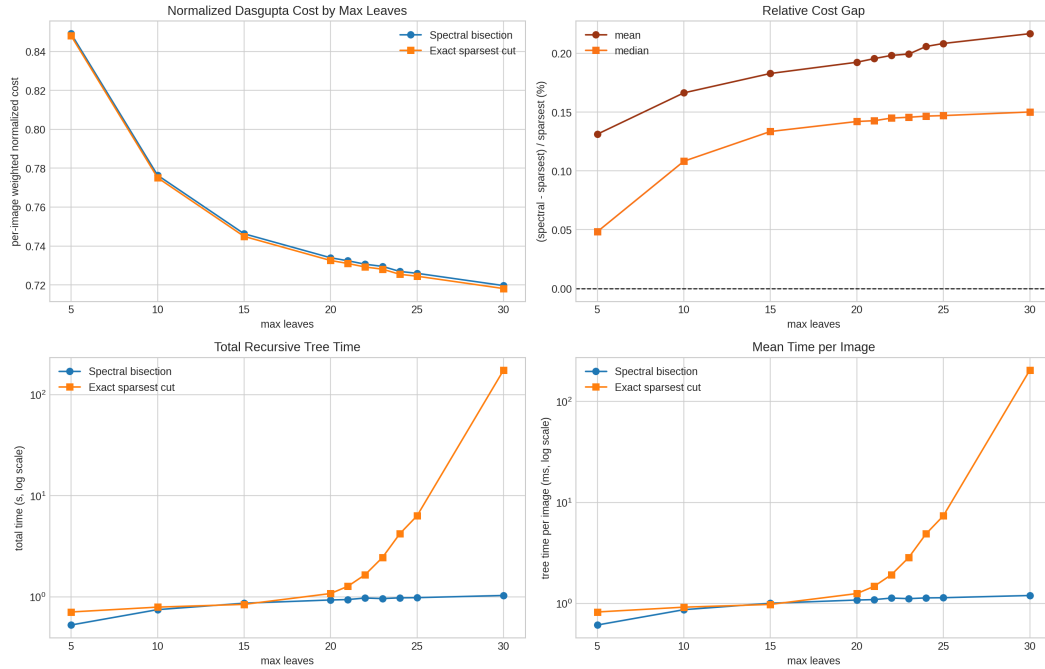


Figure 4: Comparison between recursive spectral bisection and exact recursive sparsest cut for 2D hierarchy construction. Spectral bisection closely matches the normalized Dasgupta cost of exact sparsest cut while keeping preprocessing time nearly constant. Time plots use a log scale.

remains around one second. The same trend appears in mean per-image time, where exact sparsest cut increases by orders of magnitude while spectral bisection stays nearly flat. These results support using spectral bisection as a practical surrogate: it introduces only a minor Dasgupta-cost increase but removes the main preprocessing bottleneck for dense DINO affinity graphs.